Terr. Atmos. Ocean. Sci., Vol. 23, No. 6, 633-645, December 2012 doi: 10.3319/TAO.2012.08.14.01(T)

Fluctuation Analyses of M ≥ 3 Earthquake Sequences in The Taipei Metropolitan Area

Jeen-Hwa Wang[1, *], Kou-Cheng Chen[1], Shiann-Jong Lee[1], Win-Gee Huang[1], and Pei-Ling Leu[2]

[1] *Institute of Earth Sciences, Academia Sinica, Nangang, Taipei, Taiwan*
[2] *Seismological Center, Central Weather Bureau, Taipei, Taiwan*

Received 10 April 2012, accepted 14 August 2012

ABSTRACT

The M ≥ 3 earthquakes which occurred in the Taipei Metropolitan Area from 1973 through 2010 are used to study the memory effect of earthquake sequences in the area by applying a fluctuation analysis technique in the natural time domain. The earthquakes can be divided into two groups: the first for shallow events with focal depths ranging 0 - 40 km and the second with focal depths deeper than 60 km. For both shallow and deep earthquakes, three magnitude ranges, i.e., M ≥ 3, M ≥ 3.5, and M ≥ 4, are taken into account. The calculations are also made for the events in a smaller area. Calculated results show that the exponents of the scaling law of fluctuation versus window length for all earthquakes sequences in consideration are not larger than 0.5, thus suggesting that the M ≥ 3 and M ≥ 3.5 earthquakes in the TMA are short-term corrected. On the other hand, the M ≥ 4 earthquakes are weakly corrected.

Key words: Earthquake sequence, Magnitude, Inter-event time, Long- and short-term memory effects, Fluctuation analysis

Citation: Wang, J. H., K. C. Chen, S. J. Lee, W. G. Huang, and P. L. Leu, 2012: Fluctuation analyses of M ≥ 3 earthquake sequences in the Taipei Metropolitan Area. Terr. Atmos. Ocean. Sci., 23, 633-645, doi: 10.3319/TAO.2012.08.14.01(T)

1. INTRODUCTION

Taiwan is situated in the collision boundary between the Philippine Sea plate and the Eurasian plate (Tsai et al. 1977; Wu 1978; Lin 2002). The former moves northwestward with a speed of about 8 cm yr^{-1} (Yu et al. 1997) and has subducted beneath the Eurasian plate under northern Taiwan, where the Taipei Metropolitan Area (TMA) is located. This collision causes high seismicity in the Taiwan region (Wang et al. 1983; Wang 1998; Wang and Shin 1998). The TMA is the political, economic, and cultural center of Taiwan. Hence, seismic risk mitigation rightly receives much attention. For this purpose, the seismicity of the area should be investigated thoroughly. A description of the geology of the TMA can be found in several articles (e.g., Wang-Lee and Lin 1987; Chang et al. 1998; Teng et al. 2001; Wang et al. 2006) and will not be given here.

From 1972 to 1991, the Taiwan Telemetered Seismographic Network (TTSN), sponsored by the National Science Council (NSC), was operated by the Institute of Earth Sciences (IES), Academia Sinica to monitor earthquakes in Taiwan. This network consists of 24 stations, each equipped with a vertical high-gain and analog velocity seismometer. The earthquake magnitude used by the TTSN was the duration magnitude scale. Wang (1989a) described this network in details. Since 1991, the old seismic network of Central Weather Bureau (CWB) has been upgraded and many new stations have been added to form a new network called the CWB Seismic Network (CWBSN). In 1992 the TTSN was merged into the CWBSN. The earthquake magnitude of the earthquake catalogue has been unified to be the local magnitude. A detailed description of the CWBSN can be found in Shin (1992) and Shin and Chang (2005); only a brief description is given below. At present, the CWBSN is consisted of 72 stations, each equipped with a three-component velocity seismometer. The seismograms are recorded in both high- and low-gain forms. This network provides high-quality digital earthquake data to the seismological community.

The seismicity and related seismic problems in the TMA were studied on the basis of data obtained by the TTSN, CWBSN, and several portable seismic arrays constructed by several researchers (e.g., Tsai et al. 1977; Wu

* *Corresponding author*
E-mail: jhwang@earth.sinica.edu.tw

1978; Wang et al. 1983, 1994, 2006, 2011; Wang 1988; Chen and Yeh 1991; Wang and Shin 1998; Lin 2002; Kim et al. 2005; Lin et al. 2005; Konstantinou et al. 2007). A brief review can be found in Wang (2008) and Wang et al. (2006, 2012).

Figure 1a shows the sequence of events (with magnitudes M_i, i = 1, 2, 3,..., n + 1) in a conventional time domain. The inter-event time (also denoted by inter-occurrence time in some articles) between events i and i + 1 is denoted by T_i. Wang et al. (2012) applied three statistical models, the gamma, power-law, and exponential functions, to describe the single frequency distribution of inter-event times between two consecutive events for both shallow and deep earthquakes with $M \geq 3$ in the TMA from 1973 to 2010. Numerical tests suggest that the most appropriate time interval for counting the frequency of events for statistical analysis is 10 days. Results show that among the three functions, the power-law function is the most appropriate one for describing the data points. While the exponential function is the least appropriate for describing the observations, and, thus, the time series of earthquakes in consideration are not Poissonian. The gamma function is less than the power-law function and more appropriate than the exponential function to describe the observations. The scaling exponent of the power-law function decreases linearly with an increasing lower-bound magnitude. The slope value of the regression equation is smaller for shallow earthquakes than for deep events. Meanwhile, the power-law function cannot work when the threshold magnitude is 4.2 for shallow earthquakes and 4.3 for deep events. Therefore, Wang et al. (2012) assumed that the $M \geq 3$ earthquake sequences for both shallow and deep events in the TMA show a power-law behavior. Let $n(t)$ be the number of earthquakes in an area at time t. When the changing rate of $n(t)$ at time t, $dn(t)/dt$, is controlled only by $n(t)$, the relationship between $dn(t)/dt$ and $n(t)$ can be represented by a linear 1-D difference equation: $dn/dt = -\lambda n(t)$. This equation gives a solution in the form of the exponential function, $n(t) \sim \exp(-t/\lambda)$, to show its temporal behavior. When $dn(t)/dt$ is controlled not only by $n(t)$ but also by the previous numbers, for example, $n(t - \delta t)$, a memory effect exists in earthquakes. Hence, the relationship between $dn(t)/dt$ and $n(t)$ can be represented by a non-linear 1-D differencial equation: $dn/dt = -\kappa n(t)n(t - \delta t)$. We have $dn/dt = -\kappa n^2(t)$ as δt approaches zero. This gives a solution in the form of the power-law function, $n(t) \sim \kappa t^{-1}$, to show its temporal behavior. Hence, power-law behavior of an earthquake sequence suggests the possible existence of a memory effect in earthquakes. The radical problem now is in determining whether such a memory effect is long-term or short-term corrected in the earthquakes explored in this study.

A long-term memory effect appears in several phenomena, for example, in climate (e.g., Koscielny-Bunde et al. 1998), physiology (e.g., Peng et al. 1994), and the financial market (e.g., Liu et al. 1997). Lennartz et al. (2008, 2011) also assumed the existence of a long-term memory effect in earthquakes. In order to study this type of problem, the fluctuation analysis (FA) technique (Koscielny-Bunde et al. 1998; Lennartz and Bunde 2009a) is commonly commonly chosen for use. Essentially, those phenomena are assumed to be physically critical. Recently, the natural time is considered to be a good time system to represent critical phenomena (e.g., Varotsos et al. 2004, 2005; Lennartz et al. 2008, 2011; Uyeda et al. 2009). Seismicity is also considered to be one of critical phenomena (e.g., Bak and Tang 1989; Main 1996; Turcotte 1997; Rundle et al. 2003). Hence, the temporal variation in earthquakes can be represented in natural time as demonstrated in Fig. 1b in which the earthquake sequence is denoted by the count, i, of an event. Hence, the inter-event time is just one unit for all pairs of events in the natural time domain.

In this study, we will apply the FA technique to quantify possible memory effect in the sequence of $M \geq 3$ earthquakes occurring in the TMA from 1973 to 2010. In order to explore the effect of the size of earthquakes on the memory effect, the analyses will also be made for three magnitude ranges, i.e., $M \geq 3$, $M \geq 3.5$, and $M \geq 4$, in the natural time domain.

2. DATA

Data obtained as a result of shallow earthquakes which occurred in the TMA from 1973 through 1984, Wang (1988) obtained $b = 1.33 \pm 0.13$ in the magnitude range 1.8 - 3.3. For the eastern part of TMA, Wang (1989b) observed $b = 1.21 \pm 0.01$ for the events in the magnitude range of 2.1 - 4.8 occurred during 1973 to 1985. Data obtained as a result of shallow earthquakes occurring in the Tatun Volcano Group (TVG) from 1973 through 1999, Kim et al. (2005) estimated $b = 1.22 \pm 0.05$ in a magnitude range of 2.1 - 3.5. Their results show that the earthquake data should be complete with $M > 2$ in the study area. However, only $M \geq 3$ earthquakes occurred in the area (from 121.3 to 121.9°E and 24.8 to 25.3°N) over the 1973 - 2010 span are taken into account because: (1) the ability of detecting earthquakes with $M < 3$ is lower for deep events than shallow events; and (2) based on seismic risk mitigation, $M \geq 3$ earthquakes are more significant than $M < 3$ events, because damage caused by $M < 3$ events is usually very small. The earthquake data were retrieved directly from the CWB's data base. The maximum location errors are about 2 km horizontally and 5 km vertically (Shin 1992). The location error increases with depth.

2.1 Spatial Distributions of Earthquakes

The epicenters of earthquakes used in this study are plotted in Fig. 2: open circles for shallow (0 - 40 km) earthquakes and solid circles for deep (> 60 km) events as defined

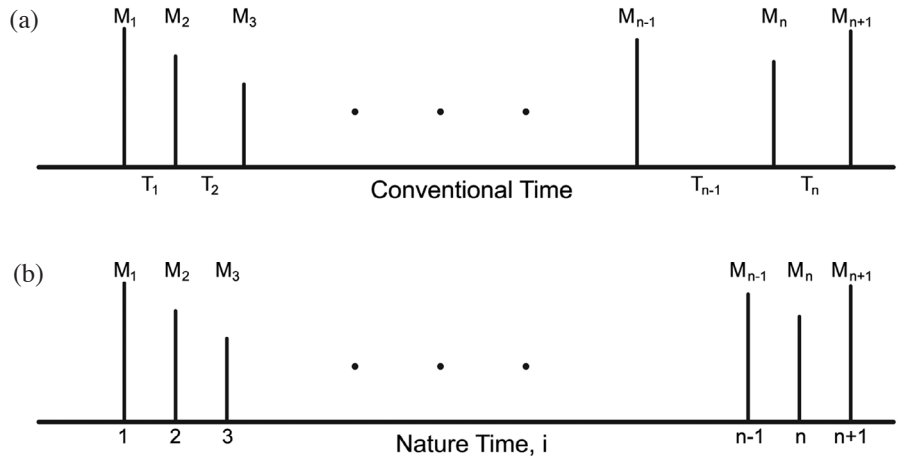

Fig. 1. Earthquake sequences: (a) displayed in the conventional time (The vertical line segments denote the magnitudes and occurrence times of earthquakes, with a time interval, T_i (i = 1, ..., n), between successive events I and i + 1; and (b) represented in the natural time, i.e., the count, i, of an event.

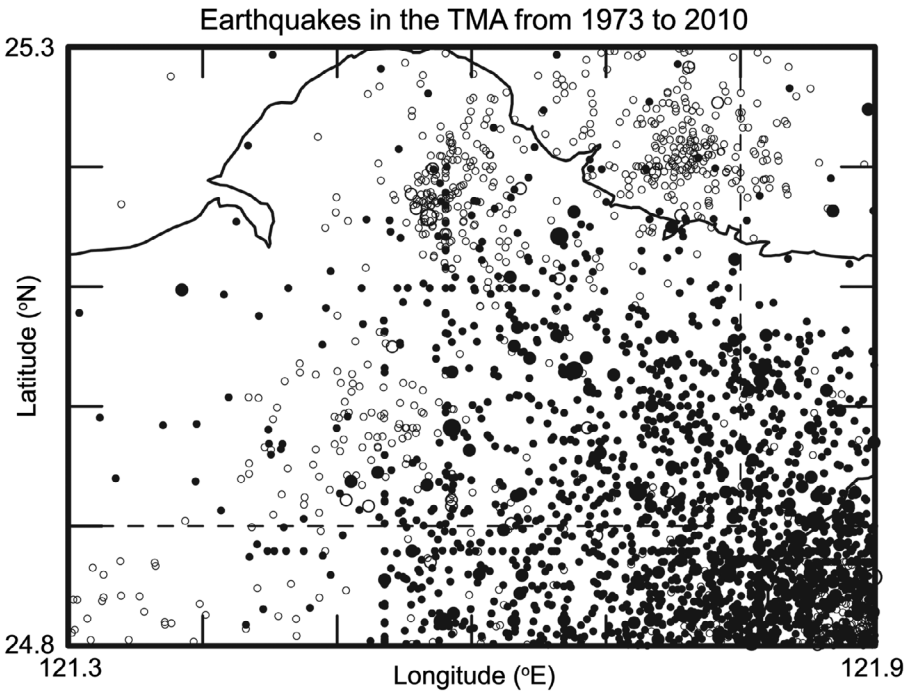

Fig. 2. Epicenters of M ≥ 3 earthquakes: open and solid circles for shallow (0 - 40 km) and deep (60 - 190 km) events, respectively. Different sizes of circles show the magnitudes of earthquakes. The dashed lines denote the upper- and lower-bounds of longitude and latitude to form a smaller area.

below. Since the location error is smaller than 5 km, the separation of the two groups of events is apparent. Figure 2 shows that deep earthquakes are located mainly to the east of 121°30'E as pointed out by Tsai et al. (1977) who suggested that the longitude of 121°30'E marks the west edge of the subduction zone. Shallow earthquakes have focal depths mainly in the range of 0 - 10 km north of 25.1°N and down to 40 km south of 25.1°N. Wang (1989b) and Wang et al. (2006) also found that the earthquakes in the eastern part of TMA can be located down to a depth of 40 km. The shallow events to the north of 25.1°N are located mainly at the TVG. Wang et al. (1994, 2006) observed that except for the earthquakes in the subduction zone, the events occurring in northern Taiwan are usually shallow. Kim et al. (2005) also obtained similar results.

Figure 3 shows the depth profile of earthquakes along a north-south profile across the TMA. Obviously, the events can be divided into two groups: one group with focal depths of 0 - 40 km and the other with focal depths > 60 km. The deep events are associated with a subducted slab. A detailed

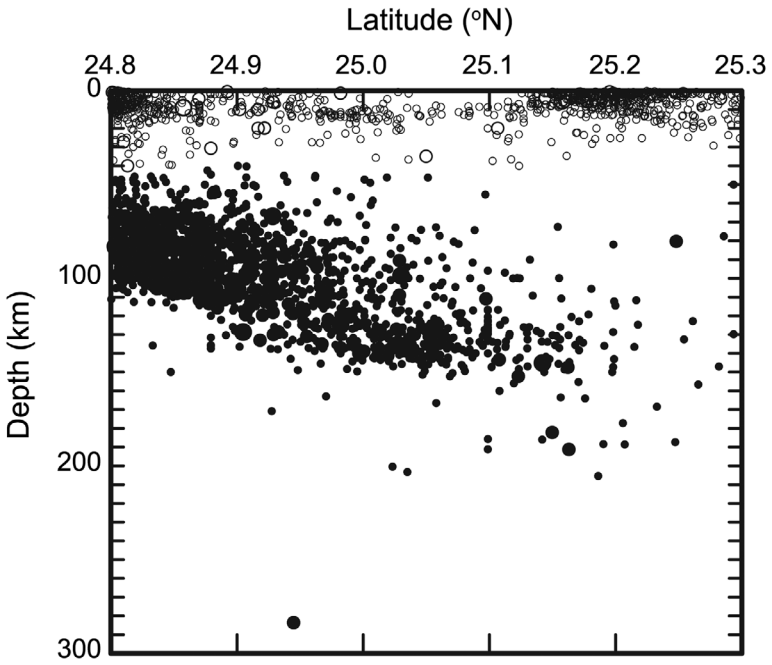

Fig. 3. Profile of earthquakes along a specific longitude (open circles for events with focal depths shallower than 40 km and solid circles for those with focal depths deeper than 40 km).

description of the depth profile can be found in Wang et al. (2006, 2012). It should be noted that the M7 earthquake of April 15, 1909 was located in the slab (Wang et al. 2011). It can be seen that an event was located at a depth of 280 km. Since the event departs away from the main trend of deep earthquakes occurring in the subduction zone, it could be miss-located. Hence, the event is not used in the following calculations. In all, 874 shallow earthquakes and 1697 deep events are used in this study. The maximum magnitudes are 5.3 and 5.7, respectively, for shallow and deep earthquakes.

2.2 Earthquake Sequences

Figure 4 shows the sequences of earthquake magnitudes in the conventional time domain (with a unit equaling one day): (a) for shallow events and (b) for deep events. The shortest inter-event times are less than 1 day for both shallow and deep earthquakes; while the longest inter-event times are 925.4 and 108.9 days, respectively, for shallow and deep events. Since some events occurred in a short time interval (for example a day) the line segments representing them cannot be clearly separated. Hence, those events are plotted by a line segment with the largest earthquake magnitude. It is obvious that after 1988 only one $M > 4$ shallow event was located in the TMA. Deep events occurred more or less uniformly in the whole study time period.

Figures 5 - 7 represent the sequences of earthquakes in the natural time domain in three magnitude ranges with different lower-bound magnitudes, M_{low}: Fig. 5 for $M \geq 3$, Fig. 6 for $M \geq 3.5$, and Fig. 7 for $M \geq 4$. In each figure, the left and right panels are made for shallow and deep events, respectively; while the upper and lower panels are plotted on the basis of magnitudes and inter-event times, respectively. The longest inter-event times are: (1) for shallow earthquakes: 925.4, 2673.9, and 6265.3 days for $M \geq 3$, $M \geq 3.5$, and $M \geq 4$, respectively; and (2) for deep earthquakes: 108.9, 410.1, and 796.3 days for $M \geq 3$, $M \geq 3.5$, and $M \geq 4$, respectively. The shortest inter-event time is smaller than 1 day for all cases. The following calculations will be

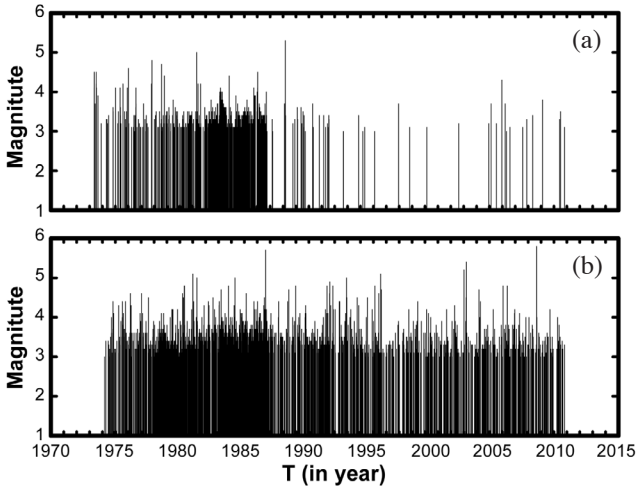

Fig. 4. Time sequences of magnitudes of $M \geq 3$ earthquakes: (a) for shallow events and (b) for deep events.

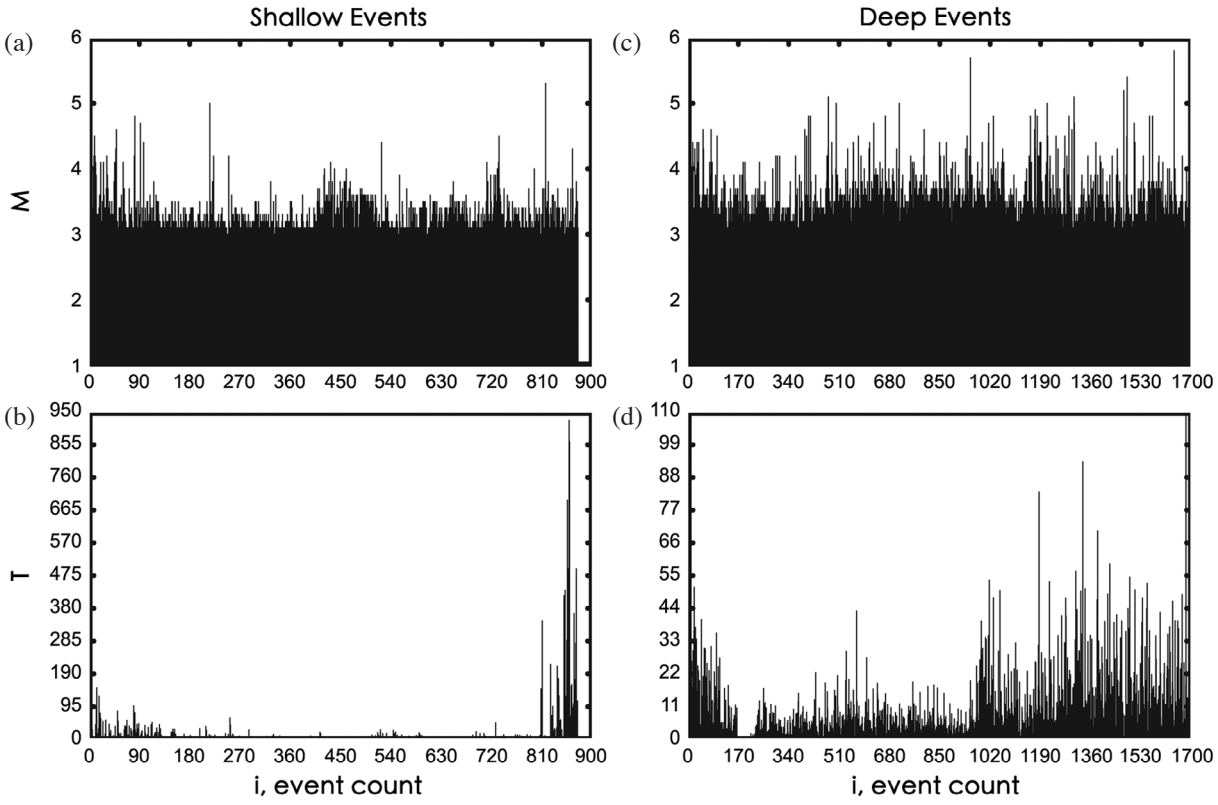

Fig. 5. The time series for M ≥ 3 earthquakes in natural time: (a) for magnitudes of shallow events; (b) for inter-event times of shallow events; (c) for magnitudes of deep events; and (d) for inter-event times of deep events.

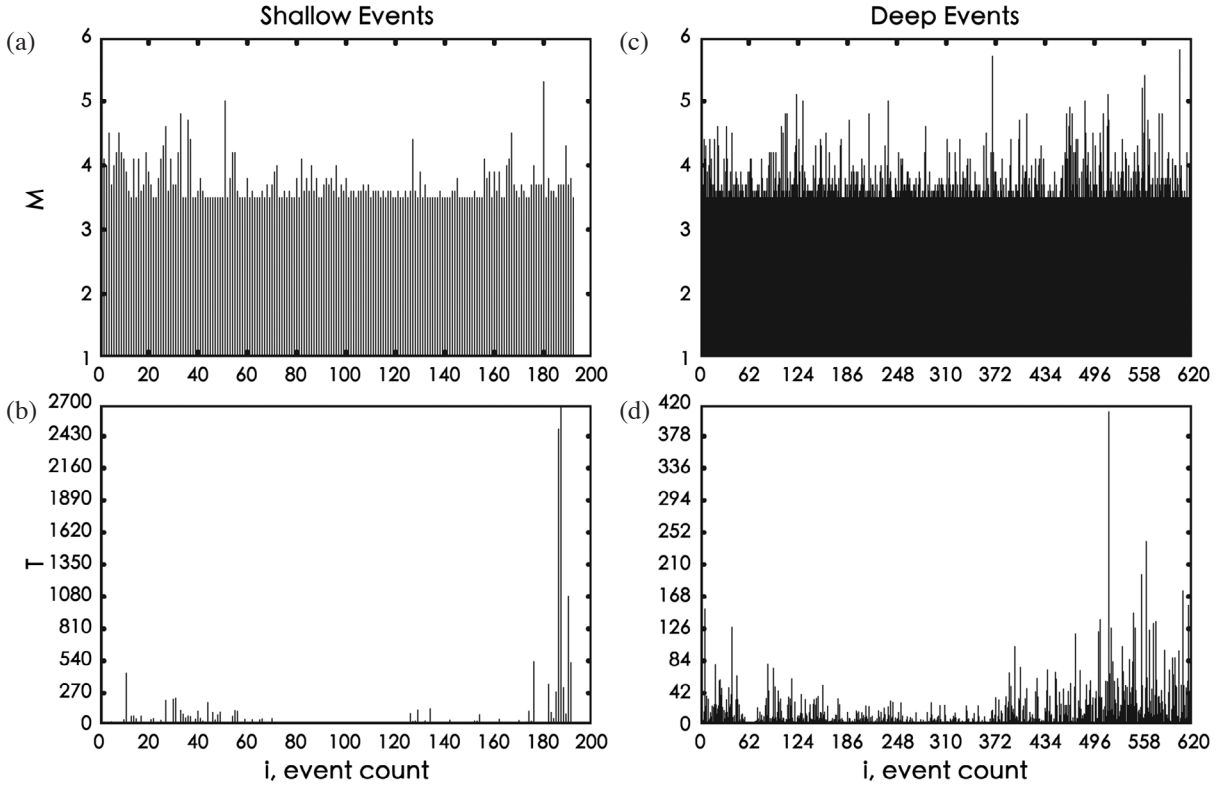

Fig. 6. The time series for M ≥ 3.5 earthquakes in natural time: (a) for magnitudes of shallow events; (b) for inter-event times of shallow events; (c) for magnitudes of deep events; and (d) for inter-event times of deep events.

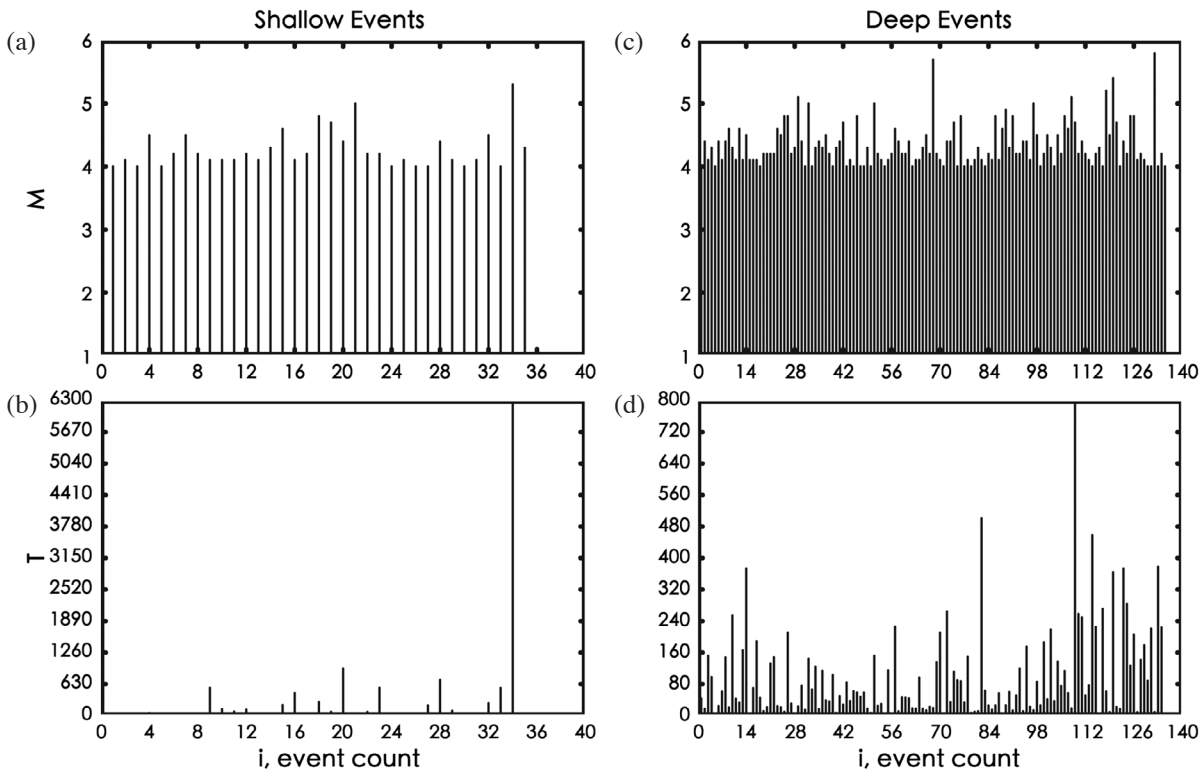

Fig. 7. The time series for M ≥ 4 earthquakes in natural time: (a) for magnitudes of shallow events; (b) for inter-event times of shallow events; (c) for magnitudes of deep events; and (d) for inter-event times of deep events.

performed based on Figs. 5 - 7. These figures show that the event variations in magnitudes are more uniform than those in inter-event times. The inter-event times are longer for lately-occurring events than for earlier-occurring ones.

3. FLUCTUATION ANALYSIS

Considering a record (x_i) of i = 1, ..., N equidistant measurements, the correlation of the values x_i and x_{i+s} for different time lags, i.e., correlations over different time scales s. In order to get rid of a constant of set in the data, the mean $\langle x \rangle$ is usually subtracted from x_i to get $y_i = x_i - \langle x \rangle$. Quantitatively, correlations between x-values separated by s steps are defined by the (auto-) correlation function: $C(s) = \langle y_i y_{i+s} \rangle$. If the x_i are uncorrelated, C(s) is zero for $s > 0$. For the short-term correlations of the x_i, C(s) decreases exponentially, $C(s) \propto \exp(-s/\sigma)$ with a decay time σ. For the long-term correlations, C(s) declines as a power-law (cf. Kantelhardta et al. 2001):

$$C(s) \propto s^{-\gamma} \qquad (1)$$

with a scaling exponent $0 < \gamma < 1$. A direct calculation of C(s) is usually not appropriate due to possible superposition of noise on the data x_i and underlying trends caused by unknown origins.

Fractional noises are defined to be a sequence of values (i.e., a time series) for which the power spectral density S(f) has a power-law dependence on frequency f. That is, (see e.g., Turcotte 1997),

$$S(f) \propto f^{-\beta} \qquad (2)$$

For an uncorrelated white noise we have a constant spectrum so that $\beta = 0$. For $\beta = 1$ we have a 1/f noise. In between, for $0 < \beta < 1$, we have long-term correlations.

In records with long-term memory a large event is more likely to be followed by a large event and a small event to be followed by a small event. This clustering leads to a "mountain-valley" structure with "mountains" and "valleys" on every time scale (Bunde et al. 2005; Livina et al. 2005; Lennartz and Bunde 2009b). The "mountain-valley" structure means that a group of a large number of events in a short time interval is followed by that of a small number of events in the sequent time interval. In addition, non-stationarities often exist in experimental and observed data. Such properties must be clearly distinguished from the intrinsic fluctuations of the system in order to find the correct scaling law of the fluctuations. This task is not easy, since, e.g., subtracting some kind of a moving average with a certain bin width would artificially introduce the time scale into the data, thus destroying a possible scaling over a wider range of time

scales. A convenient way to analyze data for long-term correlations is by using the fluctuation analysis (FA). The fluctuation function F(s) of the FA is defined as follow:

$$F^2(s) = \left\langle \left[\sum_{i=1}^{s} (x_i - \langle x \rangle) \right]^2 \right\rangle \quad (3)$$

In order to calculate the fluctuation, we first subtract from all values x_i the mean $\langle x \rangle$, where x_i is the magnitude or inter-event time at natural i. Secondly, we sum up events within a window of length s, which divide the data set (now the earthquake sequence) into several segments. If the number of events is N, the number of segments is $N_s = N/s$ where N_s is an integer. Since N is not necessary a multiple of s, the events in a small portion at the end of the sequence will not be taken in the calculations. The squared fluctuation function is then the squared sum, averaged over all windows. Accordingly, $F^2(s)$ is, up to a factor s^2, the variance of the mean values of s successive data points. For long-term correlated data sets the fluctuation function F(s) scales as

$$F(s) \propto s^{\alpha} \quad (4)$$

with $1/2 \le \alpha \le 1$. For white noise ($\beta = 0$) we have $\alpha = 1/2$, and 1/f noise ($\beta = 1$) we have $\alpha = 1$. As $\alpha < 1/2$, the data set is short-term corrected or uncorrelated. As $\alpha > 1$, the data set is non-stationary, random walk like, and unbounded. The correlation, power-spectral density and fluctuation function are related to each other by

$$\alpha = (2 - \gamma)/2 \quad (5a)$$

$$\alpha = \frac{\beta + 1}{2} \quad (5b)$$

$$\gamma = 1 - \beta \quad (5c)$$

The details concerning how to obtain the relations between the scaling exponents can be found in Kantelhardta et al. (2001) and Lennartz and Bunde (2009b). Obviously, the fluctuation function is associated with the autocorrelation function and power-spectral density. It is noted that fluctuation analysis as used here is very closely related to Hurst's rescaled-range analysis. The exponent α is equal to the Hurst exponent.

4. RESULTS

For the above-mentioned three magnitude ranges of earthquakes, the log-log plot of fluctuation F(s) [denoted by $F_M(s)$ for magnitudes and $F_T(s)$ for inter-event times] versus time window, s, are shown in Fig. 8 (symbols: open circles for M ≥ 3, crosses for M ≥ 3.5, and open squares for M ≥ 4): (a) for magnitudes of shallow events; (b) for inter-event times of shallow events; (c) for magnitudes of deep events; and (d) for inter-event times of deep events. The number of events and the maximum inter-event time for each magnitude range are given, respectively, in first parenthesis under the M-column and in that under the T-column of Table 1. Obviously, the number of events decreases and the inter-event time increases with increasing M_{low}. The value of $\log[F_M(s)]$ at each log(s) decreases with increasing M_{low}, because the number of events decreases with increasing M_{low}. On the other hand, the value of $\log[F_T(s)]$ at each log(s) increases with M_{low}, because the inter-event time increases with M_{low} even though the number of events decreases. The dashed lines denote the linear equation with a slope value of 0.5. The thin solid lines represent the inferred functions for relevant data sets and will be explained below. In Figs. 8a and c, $\log[F_T(s)]$ monotonically increases with log(s) for the three magnitude ranges. In Fig. 8b, when M ≥ 3 and M ≥ 3.5 $\log[F_T(s)]$ increases with small log(s), then falls down at log(s) = 1.279 (or s = 19) for M ≥ 3, log(s) = 0.903 (or s = 8) for M ≥ 3.5, and log(s) = 0.477 (or s = 3) for M ≥ 4, and finally increases again with log(s). In Fig. 8d, for three magnitude ranges $\log[F_T(s)]$ increases with log(s).

It is necessary to explore the possible effect on the evaluation of scaling exponent when the events occurring in an area smaller than that displayed in Fig. 2. For this purpose, the events which occurred in an area with latitudes higher than 24.9°N and longitudes smaller than 121.8°E are taken into account. This smaller area could be more appropriate to represent the TMA than the original one. The log-log plots for $F_M(s)$ and $F_T(s)$ versus time window, s, for three magnitude ranges are also made for those events and shown in Fig. 9 (symbols: open circles for M ≥ 3, crosses for M ≥ 3.5, and open squares for M ≥ 4): (a) for magnitudes of shallow events; (b) for inter-event times of shallow events; (c) for magnitudes of deep events; and (d) for inter-event times of deep events. The number of events and the maximum inter-event time for each magnitude range are given, respectively, in first parenthesis under the M-column and in that under the T-column of Table 2. Obviously, the number of events decreases and the inter-event time increases with M_{low}. A comparison between Tables 1 and 2 show that the number of events and the inter-event time are, respectively, smaller and longer for the original area than for the smaller area, and the differences between the two areas increase with M_{low}. Like Fig. 8, the value of $\log[F_M(s)]$ at each log(s) decreases with increasing M_{low}; while that of $\log[F_T(s)]$ at each log(s) increases with M_{low}. The reasons to cause the phenomena are the same as those for Fig. 8. The dashed lines denote the linear equation with a slope value of 0.5. The thin solid lines represent the inferred functions for relevant data sets and will be explained below. In Figs. 9a and c, $\log[F_M(s)]$

monotonically increases with log(s) for the three magnitude ranges. In Fig. 9b, when M ≥ 3 and M ≥ 3.5 log[F_T(s)] increases with log(s), then falls down at log(s) = 0.954 (or s = 9) for M ≥ 3 and log(s) = 0.845 (or s = 7) for M ≥ 3.5, and finally increases again with log(s). In Fig. 9d, log[F_T(s)] increases with log(s) for the three magnitude ranges.

In Figs. 8 and 9, the plots for all cases slightly become flat or show roll-over at large log(s). This might be attributed to the finite-size effect as mentioned by Lennartz and Bunde (2009b).

5. DISCUSSION

Figures 5 - 7 show that the variations in magnitude with natural time for the three magnitude ranges are quite uniform. This indicates that no abnormal earthquake happened

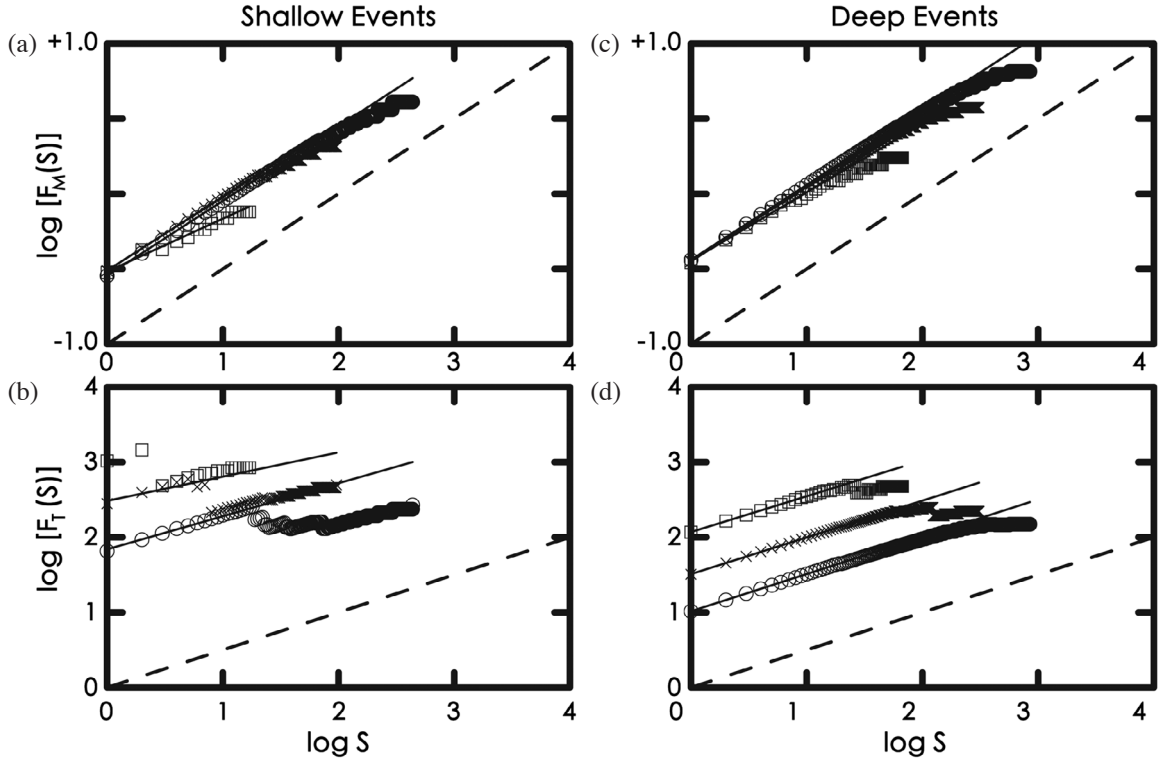

Fig. 8. The log-log plot of fluctuation F(s), versus time window, s, for M ≥ 3 (open circles), M ≥ 3.5 (crosses), and M ≥ 4 (open squares), earthquakes when all events in Fig. 2 are used: (a) for magnitudes of shallow events; (b) for inter-event times of shallow events; (c) for magnitudes of deep events; and (d) for inter-event times of deep events. The dashed lines denote the linear equation with a slope value of 0.5. The thin solid lines represent the inferred linear equations of log[F(s)] = a + α^*log(s) [F(s) = F_M(s) for magnitudes and F(s) = F_T(s) for inter-event times] from the data sets with log(s) < 1.

Table 1. The values of α^* of linear relationship between log[F(s)] and log(s), i.e., log[F(s)] = a + α^*log(s), for M ≥ 3, M ≥ 3.5, and M ≥ 4 earthquakes in two depth ranges: shallow and deep events. The values inside the first parenthesis are the number of events in the M-column and the maximum inter-event time in the T-column. The range of s for performing linear regression for each case is given in the second parenthesis.

	Shallow Events		Deep Events	
	M	**T**	**M**	**T**
M ≥ 3	(874) 0.497 ± 0.005 (1 ≤ s ≤ 10)	(925.4 days) 0.440 ± 0.028 (1 ≤ s ≤ 18)	(1697) 0.499 ± 0.002 (1 ≤ s ≤ 10)	(108.9 days) 0.496 ± 0.000 (1 ≤ s ≤ 10)
M ≥ 3.5	(192) 0.492 ± 0.001 (1 ≤ s ≤ 10)	(2673.9 days) 0.323 ± 0.069 (1 ≤ s ≤ 7)	(617) 0.497 ± 0.006 (1 ≤ s ≤ 10)	(410.1 days) 0.489 ± 0.002 (1 ≤ s ≤ 10)
M ≥ 4	(35) 0.352 ± 0.019 (1 ≤ s ≤ 10)	(6265.3 days)	(135) 0.455 ± 0.013 (1 ≤ s ≤ 10)	(796.3 days) 0.477 ± 0.003 (1 ≤ s ≤ 10)

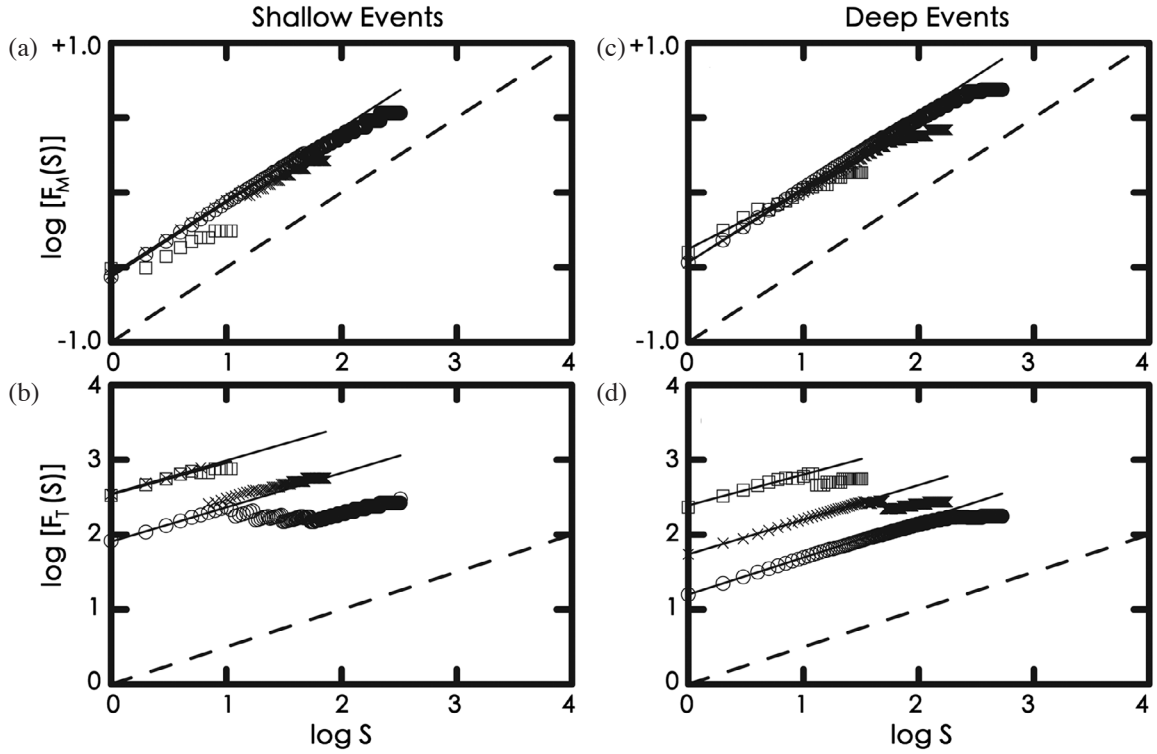

Fig. 9. The log-log plot of fluctuation F(s), versus time window, s, for M ≥ 3 (open circles), M ≥ 3.5 (crosses), and M ≥ 4 (open squares), earthquakes which occurred in a smaller area (latitudes higher than 24.9°N and longitudes smaller than 121.8°E) are used: (a) for magnitudes of shallow events; (b) for inter-event times of shallow events; (c) for magnitudes of deep events; and (d) for inter-event times of deep events. The dashed lines denote the linear equation with a slope value of 0.5. The thin solid lines represent the inferred linear equations of $\log[F(s)] = a + \alpha^* \log(s)$ [$F(s) = F_M(s)$ for magnitudes and $F(s) = F_T(s)$ for inter-event times] from the data sets with $\log(s) < 1$.

Table 2. The values of α^* of linear relationship between log[F(s)] and log(s), i.e., $\log[F(s)] = a + \alpha^* \log(s)$, for M ≥ 3, M ≥ 3.5, and M ≥ 4 events, which occurred in a smaller area (latitudes higher than 24.9°N and longitudes smaller than 121.8°E), in two depth ranges: shallow and deep earthquakes. The values inside the first parenthesis are the number of events in the M-column and the maximum inter-event time in the T-column. The range of s for performing linear regression for each case is given in the second parenthesis.

	Shallow Events		**Deep Events**	
	M	**T**	**M**	**T**
M ≥ 3	(648) 0.497 ± 0.006 (1 ≤ s ≤ 10)	(932.3 days) 0.458 ± 0.007 (1 ≤ s ≤ 8)	(1058) 0.499 ± 0.002 (1 ≤ s ≤ 10)	(133.2 days) 0.495 ± 0.001 (1 ≤ s ≤ 10)
M ≥ 3.5	(147) 0.492 ± 0.002 (1 ≤ s ≤ 10)	(2766.6 days) 0.445 ± 0.010 (1 ≤ s ≤ 6)	(357) 0.481 ± 0.008 (1 ≤ s ≤ 10)	(514.6 days) 0.463 ± 0.006 (1 ≤ s ≤ 10)
M ≥ 4	(23)	(1053.9 days) 0.424 ± 0.029 (1 ≤ s ≤ 6)	(64) 0.395 ± 0.016 (1 ≤ s ≤ 10)	(1374.7 days) 0.414 ± 0.022 (1 ≤ s ≤ 10)

in the TMA during the time period in study. On the other hand, the variations in inter-event time vary remarkably. Small inter-event time appeared in the earlier time period, while large inter-event time did in the later time period. This indicates that the frequency of earthquake occurrences was higher in the earlier time period than in the later time period. This phenomenon can also be seen in Fig. 4. The turning points appeared at 1988. This means that the TMA has been inactive since 1988. This phenomenon was first pointed out by Wang et al. (2006) and should be paid attention by local seismologists. In addition, the longest inter-event time increases with M_{low} as mentioned previously.

In Figs. 8a and c, the log-log plots of $F_M(s)$ versus s are well-distributed in three magnitude ranges for both shallow

and deep earthquakes. Figure 8b shows that the log-log plots of $F_T(s)$ versus s are ill-distributed for shallow earthquakes for the three magnitude ranges. As mentioned above, there is a significant reduction in $\log[F_T(s)]$ at a particular value of log(s): 1.279 (or s = 19) for $M \geq 3$, 0.903 (or s = 8) for $M \geq 3.5$, and 0.477 (or s = 3) for $M \geq 4.0$. Such a particular value decreases with increasing M_{low}. This might be due to a fact that when the value of log(s) is larger than the respective particular one, segmentation of an earthquake sequence results in a decrease in the number of data points due to exclusion of some data points in the later part of a sequence in calculations as mentioned above. Meanwhile, for those earthquake sequences larger inter- event times appear in the later part of a sequence as displayed in Figs. 5 - 7. This can also result in a decrease in the calculated values of $F_T(s)$. In Figs. 8a and 8b, there is no data point at large log(s) when $M \geq 4$, because the number of events is small (see Table 1). Figure 8d shows that the log-log plots of $F_T(s)$ versus s are well-distributed for deep earthquakes.

Although the ill-distributed log-log plot of $F_T(s)$ versus s for shallow earthquakes cannot give us a positive answer to the memory effect, the relevant log-log plot of $F_M(s)$ versus s as displayed in Fig. 8a can still help us to study the problem. Figure 8 seems to suggest the presence of a linear relationship between $\log[F(s)]$ [for both $F_M(s)$ and $F_T(s)$] and log(s) at small log(s). In order to perform linear regression, the linear equation represented by $\log[F(s)] = a + \alpha^* \log(s)$ is taken for the data points in a certain range of log(s), within which a linear relationship exists. The range of s for each case is shown in Table 1. Obviously, α^* is the α value for the data points in such a range of s rather than in the whole range of s in use. The values of α^* for shallow and deep earthquakes in the three magnitude ranges and vary from 0.352 to 0.499 for magnitude and from 0.323 to 0.496 for inter-event time and are given in Table 1. The standard error for the inter-event time when $M \geq 3$ is smaller than 0.001, it is given by "0.000" in Table 1.

In Fig. 9a, the log-log plots of $F_M(s)$ versus s are well-distributed for $M \geq 3$ and $M \geq 3.5$, yet not for $M \geq 4$. There is a significant reduction in $\log[F_M(s)]$ at log(s) = 0.301 (or s = 2) for $M \geq 4$. In Fig. 9b, the log-log plots are ill-distributed for $M \geq 3$ and $M \geq 3.5$ but well- distributed for $M \geq 4$. As mentioned above, there is a significant reduction in $\log[F_T(s)]$ at a particular value of log(s): 0.954 (or s = 9) for $M \geq 3$ and 0.845 (or s = 7) for $M \geq 3.5$. This reduction does not appear for $M \geq 4$. Such a particular value of log(s) decreases with increasing M_{low}. The ill-distributed patterns might be due to a reason that when the value of s is larger than the respective particular value, segmentation of an earthquake sequence results in a decrease in the number of data points due to exclusion of some data points in the later part of a sequence in calculations. Moreover, for those earthquake sequences longer inter-event times appear in the later part of a sequence as displayed in Figs. 5 - 7, and thus are not included in calculations at large log(s). This makes the calculated values of $F_T(s)$ reduce. In Figs. 9a and b there is no data point at large log(s) when $M \geq 4$, because the number of events is small (see Table 2). In Figs. 9c and d, the log-log plots are well-distributed for the three magnitude ranges.

For shallow earthquakes, the log-log plots of $F_M(s)$ versus s for $M \geq 4$ in Fig. 9a and those of $F_T(s)$ versus s for $M \geq 3$ and $M \geq 3.5$ in Fig. 9b are ill-distributed and thus cannot give us a reliable answer to the memory effect. However, the relevant log-log plot of $F_T(s)$ versus s in Fig. 9b and those of $F_M(s)$ versus s in Fig. 9a can still help us to study the problem. Figure 9 seems to suggest the presence of a linear relationship between $\log[F(s)]$ [for both $F_M(s)$ and $F_T(s)$] and log(s) at small log(s). Like Fig. 8, the linear equation, which is represented by $\log[F(s)] = a + \alpha^* \log(s)$, is inferred from the data points in a certain range of s, which is shown in Table 2, the result is displayed by a thin solid line in Fig. 9. The values of α^* in the three magnitude ranges vary from 0.395 to 0.499 for the magnitude cases and from 0.414 to 0.496 for the inter-event time cases and are given in Table 2.

Clearly, all α^* values are not larger than 0.5. For shallow earthquakes, the smallest value of α^* is 0.357 when $M \geq 4$ for the magnitude cases and 0.322 when $M \geq 3.5$ for the inter-event time cases. Almost all data points with log(s) > 1 (or s > 10) in Figs. 8 and 9 are not above the regression lines. This will lead to a fact that the average value of α^* in Eq. (3) should be smaller than 0.5 for all cases, when it is evaluated from all data points. This suggests that the memory effect in earthquakes of this study could be only short-term corrected or weakly corrected. From Figs. 8 and 9 and Tables 1 and 2, the α^* values are closer to 0.5 for the group of deep earthquakes than that of shallow events. This implies that the correlation between events is stronger for the former than for the latter. For shallow earthquakes, the α^* values are closer to 0.5 for the magnitude cases than for the inter-event time cases and the difference between them increases with M_{low}. Moreover, the α^* value cannot be calculated for the events with $M \geq 4$. Results might implicate incompleteness of the sequence of shallow events, especially for those with $M \geq 4$, in use. Meanwhile, the α^* values for the magnitude cases are close to 0.5 only when $M \geq 3$ and $M \geq 3.5$ and the value departs from 0.5 when $M \geq 4$. This suggests that as considering the sequence of magnitudes, the memory effect is operative only for the events with $M < 4$ and the events with $M \geq 4$ occur almost randomly or are only weakly-corrected.

The α^* values are in general larger for the events in the original area than for those in the smaller area. The difference between the two areas is relatively large when $M \geq 4$. Figure 2 shows that a large number of $M \geq 4$ events are located outside the smaller area, thus decreasing the number of $M \geq 4$ events when the smaller area is taken into account. Although the inter-event time is longer for the events in a smaller area, a remarkable decrease in the number of events

(see Tables 1 and 2) will make the calculated values of $F_M(s)$ and $F_T(s)$ reduce, especially at larger s, thus decreasing the value of α^*. This is mainly due to the segmentation effect on the data as mentioned before. The value of α^* decreases with increasing M_{low} for both shallow and deep earthquakes in the original and smaller areas in study. This indicates that the degree of correlation between events decreases with increasing M_{low}. This again confirms the suggestion that the degree of correlation between events decreases with increasing M_{low}.

For almost all cases, a linear correlation exists for small s, especially for $s < 10$. When M_{low} is smaller than 4, the scaling exponent is smaller but close to 0.5, thus indicating that an earthquake could be influenced by few (< 10) events occurred before it. For the same data in the TMA, Wang et al. (2012) found that it is more appropriate to use the power-law function to describe the earthquake sequences for both shallow and deep events than to use either the gamma function or the exponential function. Their results suggest the possible existence of memory effect in the earthquake sequences as mentioned previously. In addition, they also observed that the component of exponential law increases with M_{low}. This means that the degree of random of earthquake occurrences increases and that of correlation between events decreases with increasing M_{low}. The earthquakes with $M \geq 4$ in the TMA occur almost randomly. Together with their results and those of this study, we can assume that in the TMA the $M \geq 3$ earthquakes are short-term corrected and the $M \geq 4$ events are weakly corrected. Obviously, the short-term correction is operative mainly for the events with magnitudes in between 3 and 4.

The present observations are different to those obtained by Lennartzet al. (2008, 2011) for the earthquake sequences in northern and southern California, for which they assumed the existence of long-term memory effect. This might be due to a fact that many mainshock- aftershocks sequences with mainshocks of magnitudes > 6 were included in their study, while only few mainshock-aftershocks sequences with mainshocks of magnitudes < 5 are included in the present data sets (see Figs. 5 - 7). The lasting time of aftershocks increases with the size of the mainshock. This is due to strong correlations between aftershocks and their mainshock and between an aftershock with others as described by Omori law. Aftershocks are considered to be the result of stress alterations in the crust induced by mainshocks through time-dependent processes, for example, the pore-fluid flow, viscous relaxation of the lower crust and upper mantle, and afterslip. Viscoelastic relaxation is a common mechanism for generating aftershocks (Scholz 1990; Chen et al. 2012). Therefore, the memory effect should be higher and longer for the mainshoch-aftershocks sequence with a larger mainshock than that with a smaller mainshock. This is the reason why Lennartz et al. (2011) studied the scaling law of F(s) versus s from the BASS model of aftershocks (Turcotte et al. 2007). Hence, it is not surprised that the long-term corrected memory effect is not operative in the earthquake sequences in the TMA.

6. CONCLUSIONS

The $M \geq 3$ earthquakes occurred below the Taipei Metropolitan Area during 1973 - 2010 can be divided into shallow (0 - 40 km) and deep (> 60 km) earthquakes, which are located in the crust and in subduction zone, respectively. Those earthquakes are taken to study the memory effect by using the fluctuation analysis technique. The earthquake sequences are represented in the temporal variations of magnitudes and inter-event times in the natural time domain. For both shallow and deep earthquakes, three magnitude ranges, i.e., $M \geq 3$, $M \geq 3.5$, and $M \geq 4$, are also taken into account. In addition to the events of original area, those in a smaller area are also considered. Calculated results show that the values of scaling exponents of Eq. (3) for all earthquake sequences in consideration are not larger than 0.5, and the value decreases with an increase in the lower-bound magnitude. Except for $M \geq 4$ events, the scaling exponents for the smaller area are similar to those for the original study area. Results further suggest the existence of short-term corrected memory effect for smaller-sized earthquakes with a lower-bound magnitude smaller than 4 and weakly corrected for larger-sized events with a lower-bound magnitude of 4.

Acknowledgements The authors would like to thank the Central Weather Bureau for providing earthquake data. They also thank two reviewers for giving significant suggestions and comments to improve the article. This work was sponsored by Academia Sinica (Taipei) and the National Science Council under Grant No. NSC100-2119-M-001-015.

REFERENCES

Bak, P. and C. Tang, 1989: Earthquake as a self-organized critical phenomenon. *J. Geophys. Res.*, **94**, 15635-15637, doi: 10.1029/JB094iB11p15635. [Link]

Bunde, A., J. F. Eichner, J. W. Kantelhardt, and S. Havlin, 2005: Long-term memory: A natural mechanism for the clustering of extreme events and anomalous residual times in climate records. *Phys. Rev. Lett.*, **94**, 048701, doi: 10.1103/PhysRevLett.94.048701. [Link]

Chang, H. C., C. W. Lin, M. M. Chen, and S. T. Lu, 1998: An Introduction to the Active Faults of Taiwan, Explanatory Text of the Active Fault Map of Taiwan SCALE 1:55000. Central Geological Survey, MOEA, ROC, 103 pp. (in Chinese)

Chen, C. C., J. H. Wang, and W. J. Huang, 2012: Material decoupling as a mechanism of aftershock generation. *Tectonophysics*, **546-547**, 56-59, doi: 10.1016/j.tecto.2012.04.016. [Link]

Chen, K. J. and Y. H. Yeh, 1991: Gravity and microearthquake studies in the Chinshan-Tanshui area, northern Taiwan. *Terr. Atmos. Ocean. Sci.*, **2**, 35-50.

Kantelhardt, J. W., E. Koscielny-Bunde, H. H. A. Rego, S. Havlin, and A. Bunde, 2001: Detecting long-range correlations with detrended fluctuation analysis. *Physica A*, **295**, 441-454, doi: 10.1016/S0378-4371(01)00144-3. [Link]

Kim, K. H., C. H. Chang, K. F. Ma, J. M. Chiu, and K. C. Chen, 2005: Modern seismic observations in the Tatun volcano region of northern Taiwan: Seismic/volcanic hazard adjacent to the Taipei Metropolitan area. *Terr. Atmos. Ocean. Sci.*, **16**, 579-594.

Konstantinou, K. I., C. H. Lin, and W. T. Liang, 2007: Seismicity characteristics of a potentially active Quaternary volcano: The Tatun Volcano Group, northern Taiwan. *J. Volcanol. Geotherm. Res.*, **160**, 300-318, doi: 10.1016/j.jvolgeores.2006.09.009. [Link]

Koscielny-Bunde, E., A. Bunde, S. Havlin, H. E. Roman, Y. Goldreich, and H. J. Schellnhuber, 1998: Indication of a universal persistence law governing atmospheric variability. *Phys. Rev. Lett.*, **81**, 729-732, doi: 10.1103/PhysRevLett.81.729. [Link]

Lennartz, S. and A. Bunde, 2009a: Trend evaluation in records with long-term memory: Application to global warming. *Geophys. Res. Lett.*, **36**, L16706, doi: 10.1029/2009GL039516. [Link]

Lennartz, S. and A. Bunde, 2009b: Eliminating finite-size effects and detecting the amount of white noise in short records with long-term memory. *Phys. Rev. E*, **79**, 066101, 1-6, doi: 10.1103/PhysRevE.79.066101. [Link]

Lennartz, S., V. N. Livina, A. Bunde, and S. Havlin, 2008: Long-term memory in earthquakes and the distribution of interoccurrence times. *EPL*, **81**, 69001, 1-5, doi: 10.1209/0295-5075/81/69001. [Link]

Lennartz, S., A. Bunde, and D. L. Turcotte, 2011: Modelling seismic catalogues by cascade models: Do we need long-term magnitude correlations? *Geophys. J. Int.*, **184**. 1214-1222, doi: 10.1111/j.1365-246X.2010.04902.x. [Link]

Lin, C. H., 2002: Active continental subduction and crustal exhumation: The Taiwan orogeny. *Terr. Nova*, **14**, 281-287, doi: 10.1046/j.1365-3121.2002.00421.x. [Link]

Lin, C. H., 2005: Seismicity increase after the construction of the world's tallest building: An active blind fault beneath the Taipei 101. *Geophys. Res. Lett.*, **32**, L22313, doi: 10.1029/2005GL024223. [Link]

Liu, Y., P. Cizeau, M. Meyer, C. K. Peng, and H. E. Stanley, 1997: Correlations in economic time series. *Physica A.*, **245**, 437-440, doi: 10.1016/S0378-4371(97)00368-3. [Link]

Livina, V. N., S. Havlin, and A. Bunde, 2005: Memory in the occurrence of earthquakes. *Phys. Rev. Lett.*, **95**, 208501, doi: 10.1103/PhysRevLett.95.208501. [Link]

Main, I., 1996: Statistical physics, seismogenesis, and seismic hazard. *Rev. Geophys.*, **34**, 433-462, doi: 10.1029/96RG02808. [Link]

Peng, C. K., S. V. Buldyrev, S. Havlin, M. Simons, H. E. Stanley, and A. L. Goldbeger, 1994: Mosaic organization of DNA nucleotides. *Phys. Rev. E*, **49**, 1685-1689, doi: 10.1103/PhysRevE.49.1685. [Link]

Rundle, J. B., D. L. Turcotte, R. Shcherbakov, W. Klien, and C. Sammis, 2003: Statistical physics approach to understanding the multiscale dynamics of earthquake fault systems. *Rev. Geophys.*, **41**, 1019, doi: 10.1029/2003RG000135. [Link]

Scholz, C. H., 1990: The Mechanics of Earthquakes and Faulting. Cambridge University Press, New York, 439.

Shin, T. C., 1992: Some implications of Taiwan tectonic features from the data collected by the Central Weather Bureau Seismic Network. *Meteorol. Bull. CWB*, **38**, 23-48. (in Chinese)

Shin, T. C. and J. S. Chang, 2005: Earthquake monitoring systems in Taiwan. In: Wang, J. H (Ed.), The 921 Chi-Chi Major Earthquake, Office of Inter-Ministry S&T Program for Earthquake and Active-fault Research, NSC, 43-59. (in Chinese)

Teng, L. S., C. T. Lee, C. H. Peng, W. F. Chen, and C. J. Chu, 2001: Origin and geological evolution of the Taipei Basin, Northern Taiwan. *West Pac. Earth Sci.*, **1**, 115-142.

Tsai, Y. B., T. L. Teng, J. M. Chiu, and H. L. Liu, 1977: Tectonic implications of the seismicity in the Taiwan region. *Mem. Geol. Soc. China*, **2**, 13-41.

Turcotte, D. L., 1997: Fractals and Chaos in Geology and Geophysics. Cambridge University Press, Cambridge, UK, 398 pp.

Turcotte, D. L., J. R. Holliday, and J. B. Rundle, 2007: BASS, an alternative to ETAS. *Geophys. Res. Lett.*, **34**, L12303, doi: 10.1029/2007GL029696. [Link]

Uyeda, S., M. Kamogawa, and H. Tanaka, 2009: Analysis of electrical activity and seismicity in the natural time domain for the volcanic-seismic swarm activity in 2000 in the Izu Island region, Japan. *J. Geophys. Res.*, **114**, B02310, doi: 10.1029/2007JB005332. [Link]

Varotsos, P. A., N. V. Sarlis, E. S. Skordas, and M. S. Lazaridou, 2004: Entropy in the natural time domain. *Phys. Rev. E*, **70**, 011106, doi: 10.1103/PhysRevE.70.011106. [Link]

Varotsos, P. A., N. V. Sarlis, H. K. Tanaka, and E. S. Skordas, 2005: Similarity of fluctuations in correlated systems: The case of seismicity. *Phys. Rev. E*, **72**, 041103, doi: 10.1103/PhysRevE.72.041103. [Link]

Wang, C. Y. and T. C. Shin, 1998: Illustrating 100 years of Taiwan seismicity. *Terr. Atmos. Ocean. Sci.*, **9**, 589-614.

Wang, J. H., 1988: *b* values of shallow earthquakes in Taiwan. *Bull. Seismol. Soc. Am.*, **78**, 1243-1254.

Wang, J. H., 1989a: The Taiwan telemetered seismographic network. *Phys. Earth Planet. Inter.*, **58**, 9-18, doi: 10.1016/0031-9201(89)90090-3. [Link]

Wang, J. H., 1989b: Aspects of seismicity in the southernmost part of the Okinawa trough. *Proc. Geol. Soc. China*, **32**, 79-99.

Wang, J. H., 1998: Studies of earthquake seismology in Taiwan during the 1897-1996 period. *J. Geol. Soc. China*, **41**, 291-336.

Wang, J. H., 2008: Urban seismology in the Taipei metropolitan area: Review and prospective. *Terr. Atmos. Ocean. Sci.*, **19**, 213-233, doi: 10.3319/TAO.2008.19.3.213(T). [Link]

Wang, J. H., Y. B. Tsai, and K. C. Chen, 1983: Some aspects of seismicity in Taiwan region. *Bull. Inst. Earth Sci., Acad. Sin.*, **3**, 87-104.

Wang, J. H., K. C Chen, and T. Q. Lee, 1994: Depth distribution of shallow earthquakes in Taiwan. *J. Geol. Soc. China*, **37**, 125-142.

Wang, J. H., M. W. Huang, and W. G. Huang, 2006: Aspects of M ≥ 4 earthquakes in the Taipei metropolitan area. *West. Pac. Earth Sci.*, **6**, 169-190.

Wang, J. H., K. C. Chen, S. J. Lee, and W. G. Huang, 2011: The 15 April 1909 Taipei earthquake. *Terr. Atmos. Ocean. Sci.*, **22**, 91-96, doi: 10.3319/TAO.2010.08.16.01(T). [Link]

Wang, J. H., K. C. Chen, S. J. Lee, W. G. Huang, Y. H. Wu, and P. L. Leu, 2012: The frequency distribution of inter-event times of M ≥ 3 earthquakes in the Taipei metropolitan area: 1973-2010. *Terr. Atmos. Ocean. Sci.*, **23**, 269-281, doi: 10.3319/TAO.2011.12.20.01(T). [Link]

Wang-Lee, C. M. and T. P. Lin, 1987: The geology and land subsidence of the Taipei Basin. *Mem. Geol. Soc. China*, **9**, 447-464.

Wu, F. T., 1978: Recent tectonics of Taiwan. *J. Phys. Earth*, **2 (Suppl.)**, S265-S299.

Yu, S. B., H. Y. Chen, and L. C. Kuo, 1997: Velocity field of GPS stations in the Taiwan area. *Tectonophysics*, **274**, 41-59, doi: 10.1016/S0040-1951(96)00297-1. [Link]